Conference Paper

Structure and Phase Composition of Zirconium Fuel Claddings in Initial State and after Creep Tests

E. A. Kuleshova[1,2], A. S. Frolov[1], D. A. Maltsev[1], D. V. Safonov[1,2], E. V. Krikun[1], and S. V. Fedotova[1]

[1]National Research Center «Kurchatov institute», Akademika Kurchatova sqr. 1, Moscow, 123182, Russia
[2]National Research Nuclear University MEPhI (Moscow Engineering Physics Institute), Kashirskoe shosse 31, Moscow, 115409, Russia

1. Introduction

E-110 (Zr-1%Nb) zirconium alloy is used in nuclear reactors as fuel cladding material. The tightness of the fuel claddings during operation, and also during the long-term storage depends on the stability of E-110 alloy phase composition and properties [1–3]. Phase composition of Zr-based alloys is well studied [4–8], while the studies of structural evolution in Zr-1%Nb alloy under high temperature annealing and acting stresses during the creep process, as well as its influence on the processes resulting in fuel cladding integrity violation is an urgent task.

The dominant creep mechanism of zirconium alloys is dislocation climb at stresses lower than 100 MPa, and dislocation slip – at higher stresses [9]. Formation of secondary phases under prolonged static loads can also affect the strength properties of Zr alloys.

To study the structure and phase composition evolution of E-110 alloy under the influence of operational factors studies using modern high-resolution analytical equipment are necessary. These studies allow to determine not only the phase composition but also the elemental composition of the phases, and to monitor the grain texture and morphology changes during the creep process. In this paper, studies of Zr fuel cladding samples in the initial state and after creep tests were carried out.

2. Materials and research methods

To assess the structure of fuel claddings in initial state, microstructural studies of E110 alloy (Zr-1% Nb) cladding samples of two types were carried out: from electrolytic zirconium (E-Zr) and seamless cold-rolled fuel rods from sponge zirconium (S-Zr).

Corresponding Author:
D. V. Safonov
safonovdenis1993@mail.ru

Received: 21 December 2017
Accepted: 15 April 2018
Published: 6 May 2018

Publishing services provided by Knowledge E

Selection and Peer-review under the responsibility of the MIE-2017 Conference Committee.

Phase composition studies were carried out by transmission electron microscopy (TEM) using FEI Titan 80-300 transmission electron microscope and scanning electron microscopy (SEM) using a high-resolution Zeiss Merlin scanning electron microscope in heavy radioactive version.

Local inhomogeneities of the chemical composition were determined both in matrix and interphase boundaries (if any) by means of atom probe tomography (APT) using Cameca LEAP-4000 HR atom probe. Samples were prepared by electrochemical method and results were processed using Cameca IVAS 3.6.12 software.

Average grain size and texture were assessed on the samples prepared for TEM by electron backscatter diffraction (EBSD) analysis using Zeiss Merlin scanning electron microscope equipped with the Oxford Instruments Nordlys II EBSD-detector. AZtec software package was used to control the backscattered electron detector and obtain the diffraction pattern (EBSD).

The composition of the secondary phases was determined using an attachment for X-ray energy-dispersive spectroscopy (EDXS), the parameter and type of the crystal lattice was determined by the micro diffraction (SAED) method, and also by Fourier transformation [10] of HRTEM (High Resolution TEM) images identification in the Diffra-Calc software package [11].

3. Results of E110 alloy samples studies in initial state

Figure 1 (a, b) shows EBSD maps of S-Zr and E-Zr grain structure.

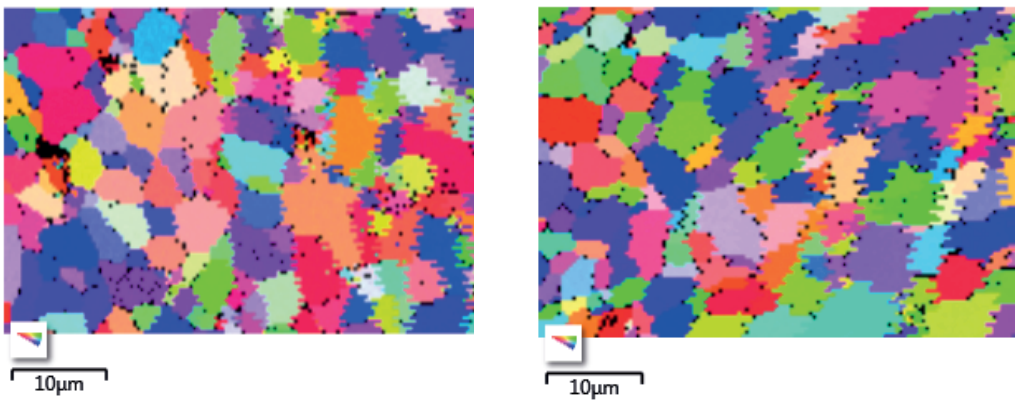

а- Г-Zr б - Э-Zr

Figure 1: EBSD-map of E110 alloy grain structure.

Grain size was determined in a plane tangent to the fuel element surface, using the chord method [1] using IVAS software. Fig. 2 (a, b) demonstrates the histograms of grain size distribution in the studied samples, and Table 1 shows the average grain

size estimation in the indicated plane, taking into account the lognormality of the distributions obtained.

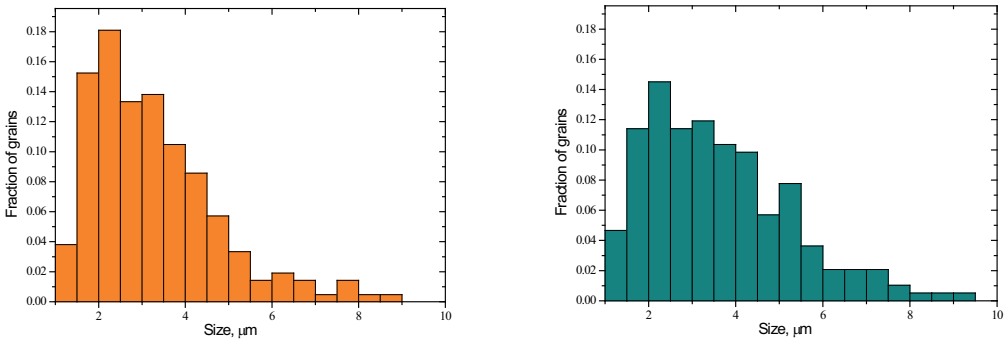

a – S-Zr b –E-Zr

Figure 2: Histograms of grain size distribution in sponge (a) and electrolytic (b) zirconium samples in the initial state.

Table 1: Grain size in the studied samples.

Material	$\overline{d}$, μm	s, μm	$CI_{95\%}$, μm
S-Zr	3.3	1.5	3.3±0.3
E-Zr	3.6	1.7	3.6±0.3

where:

- an average grain size $\overline{d} = \frac{1}{n}\sum_{i=1}^{n} d_i$, where d_i- the random value obtained in the grain size estimation, n – the number of the measured grains;
- a standard deviation: $s = \sqrt{\frac{1}{n-1}\sum_{i=1}^{n}\left(d_i - \overline{d}\right)^2}$;
- a 95% confidence interval for the average value: $CI_{95\%} = d \pm t_{2.5\%} \times \frac{s}{\sqrt{n}}$, where t_{25} - 2.5% Student distribution point.

To determine the preferential grain orientation EBSD analysis was conducted using the ring samples after electrochemical polishing in 10% perchloric acid $HClO_4$ solution in methanol CH_3OH, cooled to a temperature (minus 60 ÷ minus 50 degrees). The area of EBSD analysis for pole figures constructing was not less than 0.1 mm^2 with not higher than 1 μm step. Fig. 3 shows (0001) pole figure for sponge Zr in initial state. The texture parameters (Kearns parameters) for sponge zirconium in initial state were f_L = 0.083, f_T = 0.315, f_R = 0.602, which corresponds to the radial texture (0001) and is consistent with the literature data for the E110 alloy fuel claddings in initial state [13, 14].

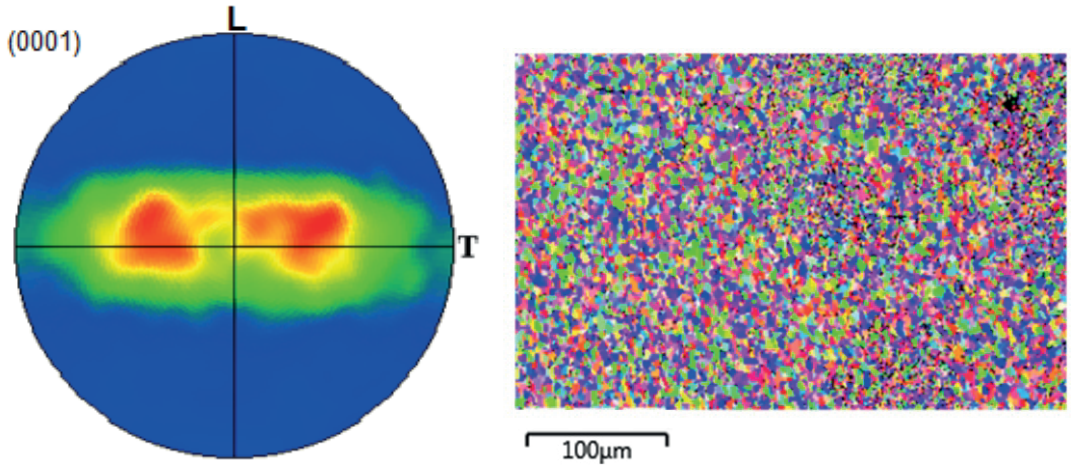

Figure 3: (0001) pole figure for sponge Zr in initial state.

TEM studies showed that dislocation structure in the fuel cladding samples in initial state is poorly developed; however some grains demonstrate the presence of dislocation networks (see Fig. 4).

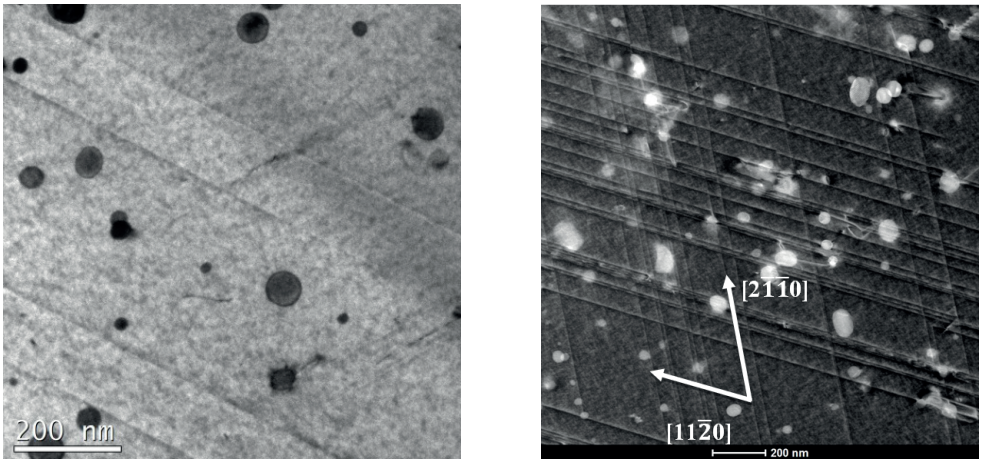

a - bright-field TEM image b - STEM-image

Figure 4: TEM-image of S-Zr sample area with dislocation networks in initial state. a - bright-field TEM image, b - STEM-image.

Such dislocation structure indicates the presence of residual plastic deformation in the studied fuel elements as a result of rolling that is in good agreement with [15], which shows the calculation results of the polycrystalline zirconium dislocation structure with a residual plastic deformation level of 0.2%.

The following phases were found in the studied S-Zr and E-Zr samples:

- rounded **β-Nb phases** with a bcc lattice (a = 3.31 Å), located predominantly in the grain body;

- **Nb-Zr–based phases** of elongated form with a fcc lattice (a = 4.35 Å) located predominantly in the grain body;
- **Zr, Nb and Fe –based phases of Zr(Nb,Fe)$_2$ type** (cubic Laves phase) with a bcc lattice (a = 3.50 Å), located in the grain body. A small amount of chromium is also present;
- **ZrH hydrides** of elongated form with a tetragonal lattice (a = 4.59 Å and c = 4.95 Å), located predominantly in the grain body.

Figure 5 (a,b,c), and 6 show typical STEM-images of secondary phases and profile of chemical element distribution in β-Nb phase.

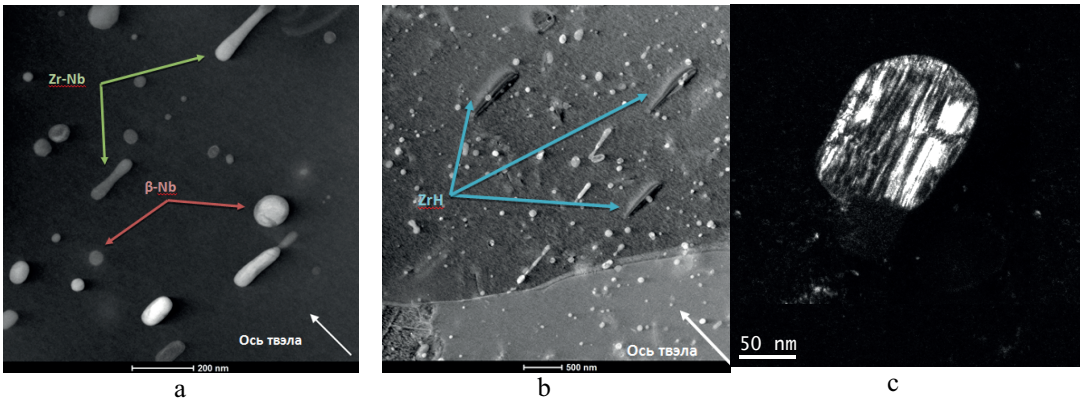

Figure 5: Dark-field STEM (a,b) and TEM (c) images of secondary phases in S-Zr sample with different magnification: β-Zr, Zr-Nb (a), ZrH hidrides (b), Zr(Nb,Fe)$_2$ Laves phase (c).

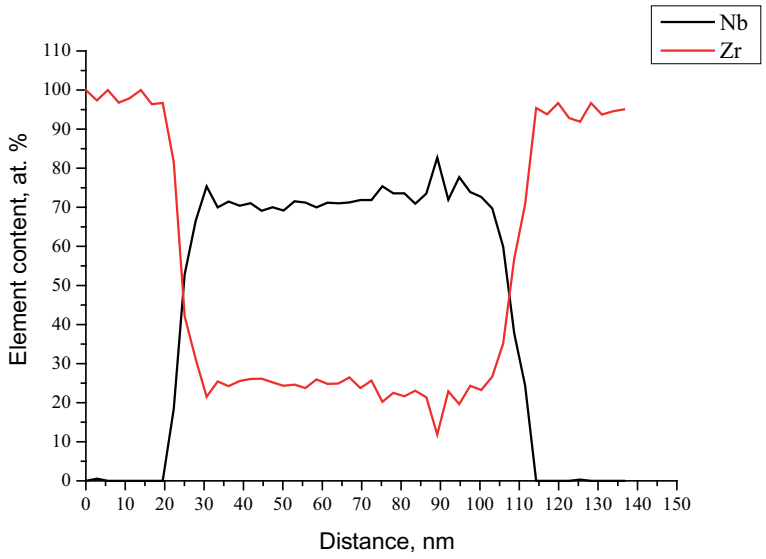

Figure 6: Typical profile of chemical element distribution for β-Nb phase in S-Zr.

The average sizes and bulk densities of the detected phases for both sponge and electrolytic zirconium are presented in Table 2. Table 3 shows the average chemical composition by EDX- analysis of the detected phases.

Table 2: The average sizes and volume densities of the secondary phases in S-Zr and E-Zr samples in initial (unirradiated) states.

Material	Secondary phases							
	β-Nb		Zr-Nb		$Zr(Nb,Fe)_2$		Zr-H	
	$\overline{d}$, nm	$\overline{\rho}$, $10^{20}m^{-3}$	$\overline{d}$, nm	$\overline{\rho}$,$10^{19}m^{-3}$	$\overline{d}$, nm	$\overline{\rho}$, $10^{19}m^{-3}$	$\overline{d}$, nm	ν, %
S-Zr	48±6	1.0±0.2	100-150	0.2-0.4	80-120	0.5-1.0	150-250	~0.01
E-Zr	34±6	1.5±0.2	100-150	0.1-0.3	80-120	0.2-0.3	150-250	~0.01

$\overline{d}$ – average size, $\overline{\rho}$ – volume density, v – volume fraction of hydrides

Table 3: The average chemical composition of phases in S-Zr and E-Zr samples in initial (unirradiated) state.

Material	Phase	Average element composition			% of the total number
		Nb	Fe	Cr	
S-Zr	β-Nb. Zr-Nb	bal.	4.9	0.0	86
	$Zr(Nb.Fe)_2$	bal.	32.2	1.4	14
E-Zr	β-Nb. Zr-Nb	bal.	8.5	0	98
	$Zr(Nb.Fe)_2$	bal.	19.0	2.7	1-2

As can be seen from Tables 2-3, in the samples studied the globular β-Nb phases with an average size of ~ 40 nm and located predominantly in the grain body has the highest density (which well agrees with the data presented in [4-8]). Besides the above phases, in the studied cladding samples based on both sponge and electrolytic Zr the elongated Zr-Nb phases were found, which previously was not mentioned in research papers. The $Nb_{0.81}Zr_{0.19}$ phase (fcc lattice, Fm-3m (225) spacing group, period 4.350Å [16]) best fits the data obtained. Fig. 7 shows the typical HRTEM-image of the Zr-Nb phase area and the corresponding Fourier transform with post-processing in the DiffraCalc software package. Figs 8-10 show similar images for the β-Nb, Zr $(Nb, Fe)_2$ phases and ZrH hydrides.

In the equilibrium state, the structure of the E110 alloy consists of α-solid solution of niobium in zirconium, in which β-Nb particles are located. Under different conditions of thermomechanical treatment, the β-Zr phase and the metastable ω-phase can be formed [17]. However, no β-Zr precipitates have been found in the structure of the

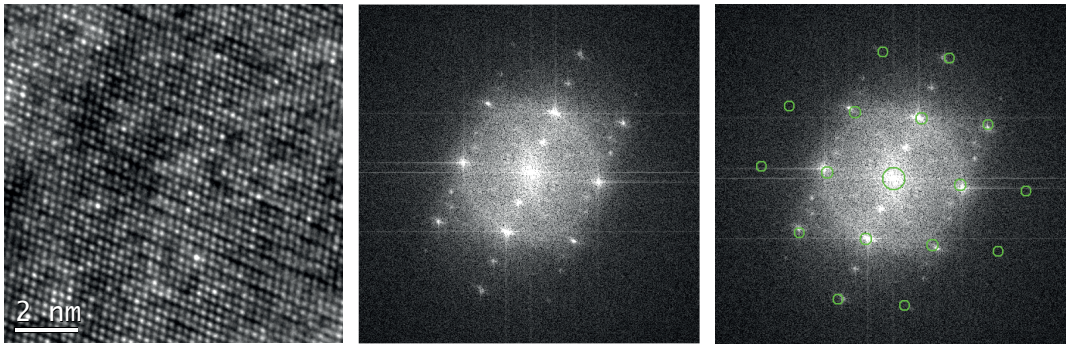

Figure 7: HRTEM-image of the Zr-Nb phase area (a) and corresponding Fourier transform (b) with post-processing in the DiffraCalc software package (Zone axis [10-1] (c)).

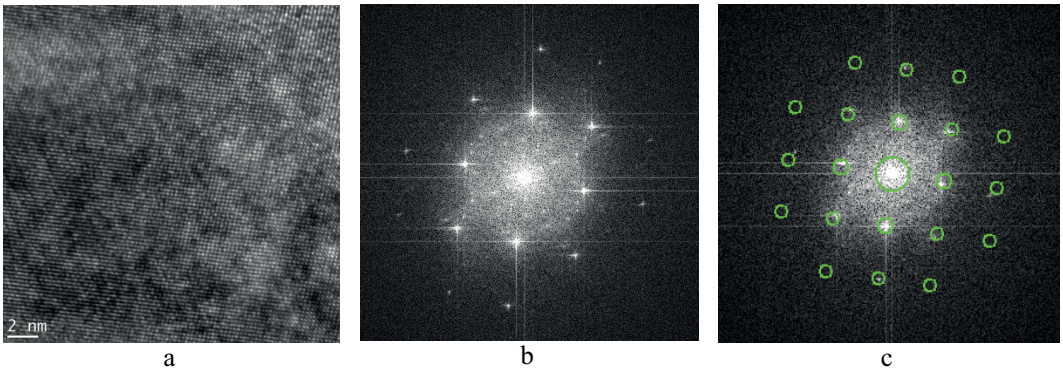

Figure 8: HRTEM- image of the β-Nb phase area (a) and corresponding Fourier transform (b) with post-processing in the DiffraCalc software package (Zone axis [100] (c)).

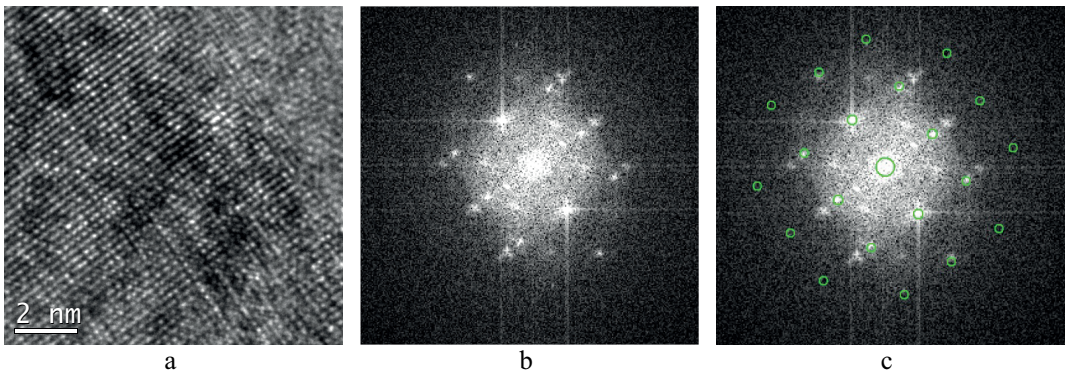

Figure 9: HRTEM- image of the $Zr(Nb,Fe)_2$ phase area (a) and corresponding Fourier transform (b) with post-processing in the DiffraCalc software package (Zone axis [100] (c)).

studied samples, which corresponds to numerous earlier studies [17-20], and this is a consequence of the technological process development of the alloy E110 manufacture.

Table 4 presents the APT-measured matrix composition of investigated samples of the fuel claddings based on both sponge and electrolytic zirconium.

According to Table 4 data, matrix contains a minor Nb amount, the rest is in a bound state - in the form of β-Nb phase, which is confirmed by microstructural studies.

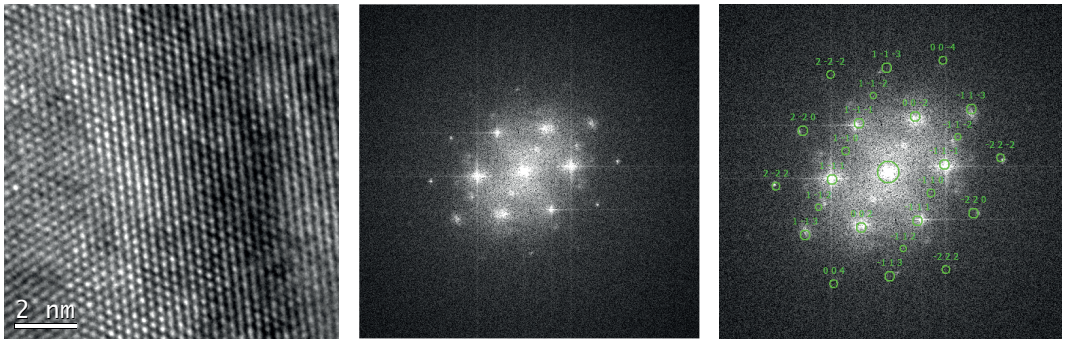

Figure 10: HRTEM- image of the ZrH hydride area (a) and corresponding Fourier transform (b) with post-processing in the DiffraCalc software package (Zone axis [10-1] (c)).

Table 4: APT-measured matrix composition of investigated fuel cladding samples.

Chemical element	Content, at.%	
	S-Zr	E-Zr
Zr	98.8	98.2
Nb	0.2	0.4
O	0.6	0.8
H	0.3	0.5
C	0.05	0.1

Fig. 11 shows APT 3D-map of chemical elements distribution from the area of E-Zr sample with Laves phase and ZrH hydride.

4. Results of E110 alloy samples studies after creep tests

The tube sample made from E110 alloy (from sponge Zr) was subjected to creep tests. The total applied load during the test was ~1200 N, which corresponds to the axial stress of 75 MPa in the working part of the sample at the initial stage of creep test. The entire creep test duration at temperature ~ 400°C was ~ 850 hours.

From the central part of the sample after creep tests, 12 mm long blanks were cut TEM samples preparation.

TEM studies showed that after creep tests phase composition of S-Zr and E-Zr is the same as for initial state.

Fig. 12a shows a (0001) pole figure of of E110 alloy sample based on sponge zirconium after creep tests. The texture parameters in this case were: F_L = 0.046, F_R = 0.615 and F_T = 0.338 (see Figure 8b). Comparison of the Kaerns parameters and (0001) pole

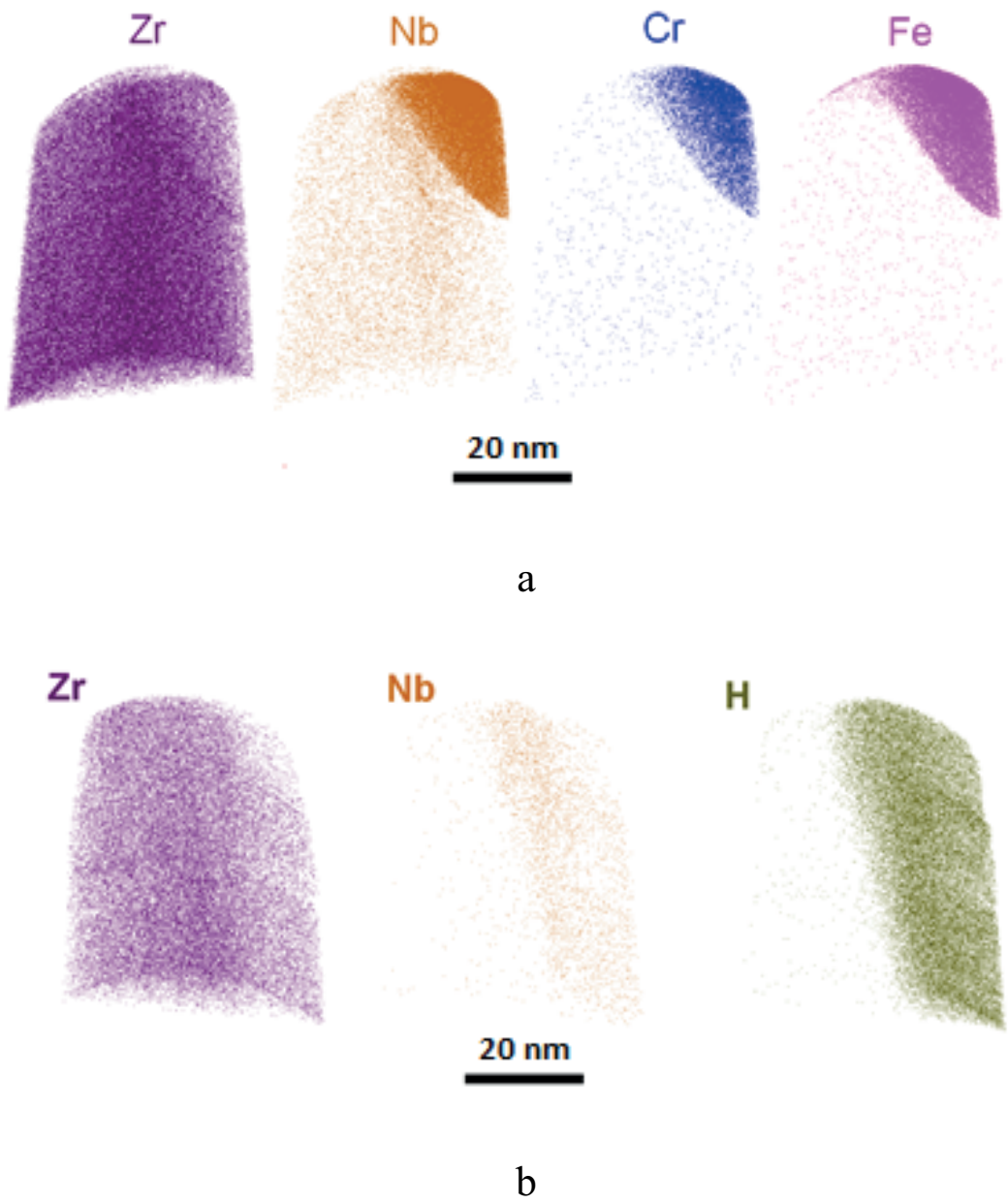

Figure 11: APT 3D-map of chemical elements distribution from the area of E-Zr sample with Laves phase (a) and ZrH hydride (b).

figures in the initial state and after the creep tests shows that the creep tests led to some change in texture parameters and the peak position on (0001) pole figures: there is an insignificant decrease in the texture maximum blurring along the axial direction and its divergence along tangential direction.

Fig. 13 illustrates that dislocations are also actively formed in this creep stage.

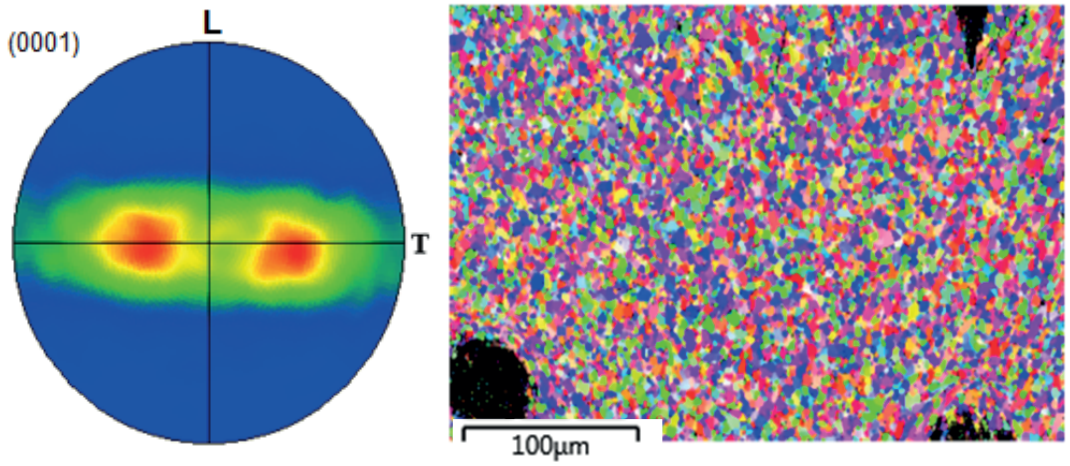

Figure 12: Results of EBSD-analysis of S-Zr sample texture after creep tests: (0001) pole figure (a), grain structure (b).

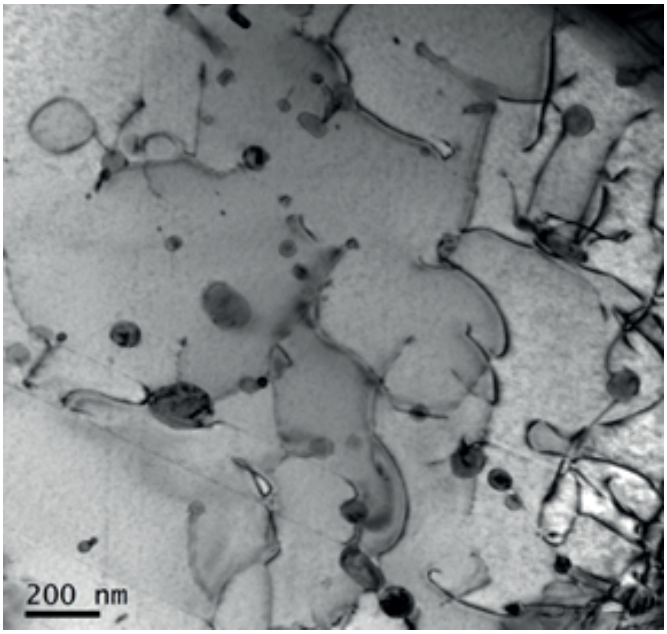

Figure 13: Bright-filed TEM-image of the S-Zr sample area after creep tests.

5. Conclusion

Quantitative structural studies of the samples of cladding fragments based on electrolytic and sponge zirconium were carried by TEM, SEM and APT methods out in initial state, including:

- grain size and texture determination by EBSD patterns obtained using the electron backscattered diffraction detector;

- phase composition studies of Zr alloys with determination of the sizes, atomic composition and types of secondary phases. For the nanoscale phase visualization STEM and APT methods were used;
- the following secondary phases were observed in the studied samples of electrolytic and sponge zirconium: β-Nb phases, niobium and zirconium based phases (Nb-Zr) with fcc lattice, zirconium, niobium and iron phases of $Zr(Nb,Fe)_2$ type (cubic Laves phase), ZrH hydrides;
- EBSD studies showed that the creep tests led to some change in texture parameters and the peak position on (0001) pole figures: there is an insignificant decrease in the texture maxinum blurring along the axial direction and its divergence along tangential direction.

References

[1] Romanato L.S. Advantages of Dry Hardened Cask Storage Over Wet Storage for Spent Nuclear Fuel // 2011 Int. Nucl. Atl. Conf. - Ina. 2011 Belo Horizonte,MG, Brazil, Oct. 24-28, 2011 Assoc. Bras. Energ. Nucl. - ABEN. 2011.

[2] Desgranges L. et al. Behavior of a defective nuclear fuel rod in dry storage conditions studied with a new experimental setup // Nucl. Technol. 2008. Vol. 163, № 2. P. 252–260.

[3] INTERNATIONAL ATOMIC ENERGY AGENCY. WWER-440 Fuel Rod Experiments Under Simulated Dry Storage Conditions. Vienna: INTERNATIONAL ATOMIC ENERGY AGENCY, 2004.

[4] Kobilyanskyi G.P. et al. Radiation damage of alloy E635 in structural elements of FA of WWER-1000 // VANT. 2009. Vol. 5. P. 57–68.

[5] Markelov V.A. On correlation of composition, structural-phase state, and properties of E635 zirconium alloy // Inorg. Mater. Appl. Res. 2010. Vol. 1, № 3. P. 245–253.

[6] Doriot S. et al. Transmission electron microscopy study of second phase particles irradiated by 2 MeV protons at 350 °C in Zr alloys // J. Nucl. Mater. Elsevier B.V, 2017. Vol. 494. P. 398–410.

[7] Bair J., Asle Zaeem M., Tonks M. A review on hydride precipitation in zirconium alloys // J. Nucl. Mater. Elsevier B.V., 2015. Vol. 466. P. 12–20.

[8] Kim H.G. et al. Corrosion and microstructural characteristics of Zr-Nb alloys with different Nb contents // J. Nucl. Mater. 2008. Vol. 373, № 1–3. P. 429–432.

[9] T.P. Chernyayeva, V.M. Grytsyna. Characteristics of HCP metals determining their behavior under mechanical, thermal and radiation exposure // Problems of atomic

science and technology. Series Physics of Radiation Damage and Radiation Material Science. 2008. Vol. 2. P. 15–27.

[10] Williams D.B., Carter C.B. Transmission Electron Microscopy: A Textbook for Materials Science. Springer, 2009.

[11] Frolov A.S. et al. Development of the DIFFRACALC software for analyzing the phase composition of alloys // Crystallogr. Reports. 2017. Vol. 62, № 5.

[12] GOST 5639-82, Steel and alloys. Methods for detection and determination of grain size.

[13] Kobylanski G.P., Shamardin V.K., Ostrovsky Z.E. et. al. Radiation shaping of shell and channel tubes from zirconium alloys at high neutron fluences // Radiation Material Science: Proceedings of the International Conference on Radiation Material Science

[14] Prasolov P.F., Shestak V.E., Platonov P.A. et. al. Anisotropy of the elasticity modulus and the coefficient of thermal expansion of textured zirconium alloys H-1 and H-2,5 // Atomic energy. 1990. V.68. I.2. P.98-101.

[15] Monnet G., Devincre B., Kubin L.P. Dislocation study of prismatic slip systems and their interactions in hexagonal close packed metals: Application to zirconium // Acta Mater. 2004. Vol. 52, № 14. P. 4317–4328.

[16] Search H. et al. Non-equilibrium solid phases formed by ion mixing in the Zr-Nb system with positive heat of formation // Mater. Sci. 1994. Vol. 39. P. 1–5.

[17] Petelguzov I.A. The influence of annealing after quenching E110 and E125 alloys on their corrosion stability // Problems of atomic science and technology. 2003. Vol. 6, № 84. P. 55–60.

[18] Stukalov A.I. Structural-phase state of Zr-2.5%Nb alloy after microwave heat treatment // Problems of atomic science and technology. 2000. Vol. 78, № 6. P. 105–119.

[19] Neklyudov I.M. et al. Research of the fuel pipes microstructure, made of calcium-thermal alloy Zr1Nb (KTC-110) // Problems of atomic science and technology.. 2002. № 82. P. 106–112.

[20] T.P. Chernyayeva. et al. The structure features of quenched alloys Zr-Nb // Problems of atomic science and technology. Physics of Radiation Damage and Radiation Material Science 2011. Vol. 2, № (97). P. 95–107.